American Mineralogist, Volume 80, pages 1104–1115, 1995

Derivation and identification of nonstandard serpentine polytypes

STURGES W. BAILEY,† JILLIAN F. BANFIELD
Department of Geology and Geophysics, University of Wisconsin–Madison, 1215 West Dayton Street, Madison, Wisconsin 53706, U.S.A.

ABSTRACT

Nonstandard trioctahedral serpentine polytypes are proving to be abundant, at least on a submicroscopic scale. These nonstandard polytypes have intermixing within the same crystal of either zero and $\pm\mathbf{b}/3$ interlayer shifts or $-\mathbf{b}/3$ and $+\mathbf{b}/3$ shifts in patterns other than $-,+,-,+$, neither of which occurs in the 12 standard polytypes. They may also have more complex ordered sequences along **c** of occupation of the two sets of octahedral cation positions not found in the standard polytypes. All possible nonstandard, interlayer shift sequences and octahedral cation sequences up to nine layers were generated by a computer program. Diffraction patterns were calculated for all sequences with periodicities encountered in our studies of natural serpentines to date (regular-stacking sequences up to four layers and ordered octahedral sequences up to seven layers). Thirty-two theoretical, nonstandard, regular-stacking polytype models are reported here. They consist of 14 regular interlayer stacking sequences (one two-layer, four three-layer, and nine four-layer) and four ordered octahedral cation sequences. The nine four-layer regular-stacking sequences can each exist with any of three possible ordered octahedral cation sequences along **c** (I,II,I,II, I,I,I,II, or I,I,II,II). Most of the nonstandard regular-stacking polytypes have triclinic geometry and $C\bar{1}$ symmetry. Two have monoclinic Cc symmetry, and in one of these **a** and **b** are reversed.

Assuming no $\mathbf{a}/3$ interlayer shifts, the octahedral cation sequence present in any polytype up to seven layers can be identified by the periodicities and intensities of the $20l$ reflections. The regular interlayer stacking sequences up to four layers can be identified uniquely by the α angle and the intensities of specific $02l$ reflections. Although it may not be known which of the pseudohexagonal $\mathbf{a}^*$ or $\mathbf{b}^*$ axes is present along with $\mathbf{c}^*$ on a given diffraction pattern, identification is possible by assuming that true $\mathbf{a}^*$ or $\mathbf{b}^*$ is present and using prescribed identification rules. We report intensities suitable for both X-ray and electron diffraction analysis. We have determined that the distortional and compositional differences likely to be encountered in natural serpentines are not great enough to obscure the diffraction characteristics that we recommend for identification.

INTRODUCTION

Polytypism is possible in hydrous phyllosilicates based on planar 1:1 layers because of two structural variables. First, cations in the octahedral sheets can occupy either of two possible sets of positions, termed I and II, which are defined as shown in Figure 1a. With $+\mathbf{a}_1$ pointing toward the viewer, the three octahedral sites around the inner OH group of each six-membered ring form a triangle pointing toward the viewer for set I and away from the viewer for set II. Because set I changes to set II by 180° or ±60° rotation about $\mathbf{c}^*$, these sets are different only when occupied in different layers, in which case the octahedral slants are in different directions (Fig. 1b). The different sets can also be described by rotations. The octahedral cations in the great majority of 1:1 layer silicates have either the same set of octahedral positions occupied in every layer or a regular alternation of the two sets in adjacent layers (I,II,I,II, etc.). Adjacent planar layers are always positioned one above the other so that there is a close pairing of each OH group on the top surface of one layer with an O atom on the basal surface of the above layer, for the orientations used here with the octahedral sheet above the tetrahedral sheet, forming long H bonds (2.7–3.2 Å between the centers of the anions). The second structural variable that makes polytypism possible is that several relative positions of adjacent layers can cause similar O-OH pairings. The six-membered rings of adjacent layers can superimpose exactly along **c** (zero shift). Alternatively, the rings can shift by $\pm\mathbf{a}/3$ along any of the three pseudohexagonal **a** axes of the structure (the sense of the shift determined by the slant of the underlying octahedra) or by $\pm\mathbf{b}/3$ along any of the three pseudohexagonal **b** axes (normal to the three **a** axes).

Theoretical stacking sequences (polytypes) for trioctahedral 1:1 layer silicates were derived by Zvyagin (1962), Steadman (1964), Zvyagin et al. (1966), Bailey (1969),

† Deceased November 30, 1994.

0003–004X/95/1112–1104$02.00

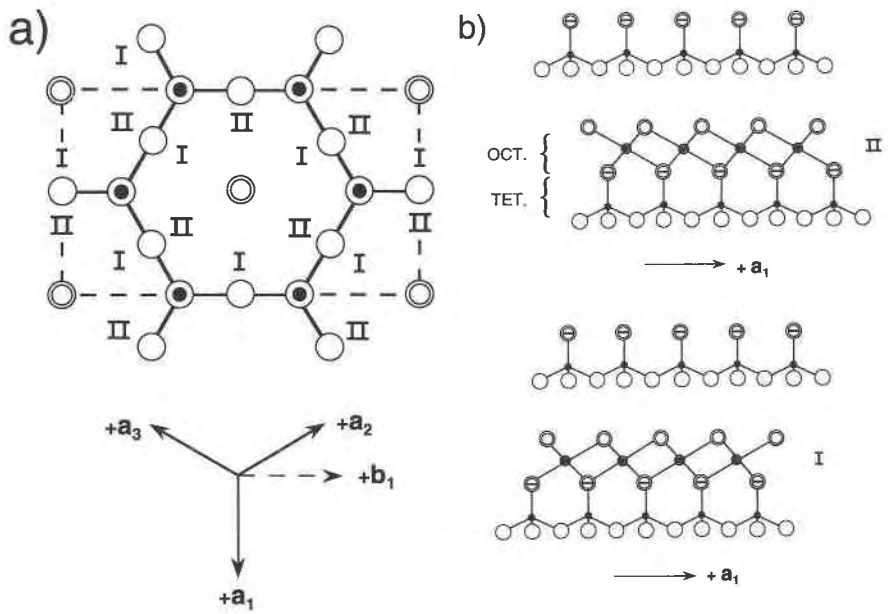

Fig. 1. Diagram illustrating (**a**) type I vs. type II octahedral sites and (**b**) polyhedral slants associated with type I vs. type II octahedral sites. Open circles represent O, double circles represent OH, and solid circles represent Si.

Dornberger-Schiff and Ďurović (1975a, 1975b), Ďurović et al. (1981), and Hall et al. (1976). All these derivations included certain simplifying assumptions that restricted the number of polytypes involved to those thought to exist in nature. For example, Steadman (1964) assumed that interlayer shifts along **a** are never accompanied by layer rotations, nor are shifts along **a** intermixed with shifts along **b**. All the other authors allowed rotation but did not allow intermixing of shifts along **a** with shifts along **b** or with zero shifts in the same crystal. Without these simplifying assumptions, many theoretical polytypes would be possible. The treatments by Dornberger-Schiff and Ďurović (1975a, 1975b) and by Ďurović et al. (1981) differed from the others by the application of OD (order-disorder) theory to 1:1 structures. Instead of treating a 1:1 layer as a combination of tetrahedral and octahedral sheets, these authors considered a 1:1 layer as an OD packet consisting of three OD layers, namely the entire tetrahedral sheet (including the inner OH groups), the plane of octahedral cations, and the plane of surface OH groups. OD theory involves all possible interrelations of the symmetry operators present in the three kinds of OD layers and in the OD packet.

The net results of the application of OD theory for trioctahedral species are identical to those of the derivations involving physical shifts of layers plus rotations (equivalent to occupation of I and II sets of octahedral positions). There are 12 so-called standard polytypes with periodicities between one and six layers along **c**, and these are equivalent to the 12 MDO (maximum degree of order) polytypes of Dornberger-Schiff and Ďurović (1975a, 1975b). The derivation of Bailey (1969) divided the 12 polytypes into four groups. Groups A and B have interlayer shifts of $\pm\mathbf{a}/3$ along the three pseudohexagonal **a** axes. Group A (polytypes $1M$, $2M_1$, and $3T$) has octahedral cations in the same set of positions in every layer, whereas group B ($2Or$, $2M_2$, and $6H$) has regular alternation of octahedral cations between sets I and II in adjacent layers. Groups C and D have shifts of $\pm\mathbf{b}/3$ along $\mathbf{b}_1$ or zero shifts (but not intermixed in the same crystal). Shifts of $\pm\mathbf{b}/3$ along $\mathbf{b}_2$ and $\mathbf{b}_3$ do not lead to additional polytypes. Group C ($1T$, $2T$, and $3R$) has octahedral cations in the same set of positions in every layer, whereas group D ($2H_1$, $2H_2$, and $6R_1$) alternates octahedral cations regularly between sets I and II. The polytypes involving zero shifts are $1T$ in group C and $2H_1$ in group D. Groups C and D are judged to have more structural stability than groups A and B and are more abundant in nature.

As far as the present authors are aware, the only report of a serpentine in which interlayer shifts along **a** are intermixed with shifts along **b** in the same crystal is that of Jahanbagloo and Zoltai (1968). On the other hand, several known natural occurrences have zero shifts intermixed with $\pm\mathbf{b}/3$ shifts along **b** in the same crystal. The most abundant of these nonstandard polytypes, designated $6R_2$ by Hall et al. (1976), has a sequence of interlayer shifts 0, $-\mathbf{b}/3$, 0, $-\mathbf{b}/3$, 0, $-\mathbf{b}/3$, with alternation of octahedral sites I and II in adjacent layers. This polytype was identified in amesite from the Northern Urals and in cronstedtite from several localities by Steadman and Nuttall (1962, 1963, 1964). Anderson and Bailey (1981) also reported $6R_2$ in amesite from the Northern Urals, and Zheng and Bailey (1995) reported it from amesite from Postmasburg, South Africa. Although the ideal symmetry of this rhombohedral six-layer structure is $R3$, Wiewióra et al. (1991) found that cation ordering decreased the symmetry to triclinic $P1$ (on hexagonal axes) for amesite from Mount Sobotka, Poland, to form a two-layer struc-

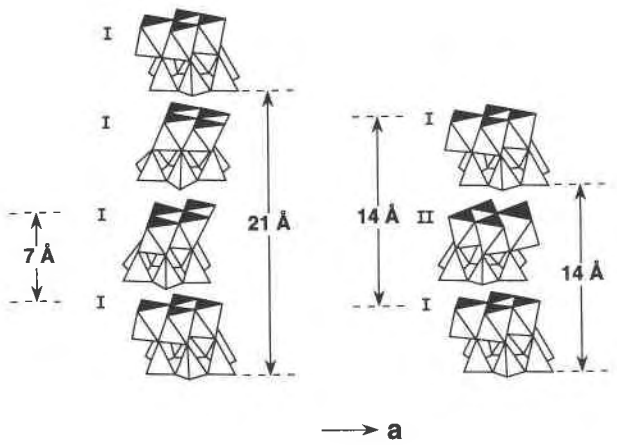

Fig. 2. Diagram illustrating that the repeat between octahedral cation planes need not be the same as that between basal O planes.

ture with $\alpha = 102°$. This is similar to nacrite, in which ordering of $^{[6]}$Al and vacancies reduces the ideal $R3c$ symmetry of the $6R_1$ polytype to monoclinic Cc to form a two-layer structure with $\beta = 114°$ (**a** and **b** reversed). Hall et al. (1976) described a second nonstandard polytype with intermixed zero and **b**/3 interlayer shifts and regular alternation of I and II octahedral site occupancies in serpentine from Unst in the Shetland Islands and in synthetic Ge- and Mg-containing serpentine described by Zussman and Brindley (1957). Hall et al. derived all possible six-layered polytypes with orthohexagonal unit cells ($\alpha = \beta = \gamma = 90°$) and both intermixing of zero and $\pm$**b**/3 interlayer shifts and regular alternation of I and II sets of octahedral positions. They designated the best-fit model as polytype $6T_1$ of ideal symmetry $P3$ (on hexagonal axes), in which the interlayer shifts are $-$**b**/3, $+$**b**/3, $-$**b**/3, $+$**b**/3, 0, 0. Subsequent work has revealed that the Unst serpentine is polygonal, and that each polygonal fiber consists of several polytypes (Banfield et al., in preparation).

We found long-period, nonstandard serpentine polytypes to be abundant when small areas are studied by selected-area electron diffraction (SAED). These might not be detected by conventional X-ray study of larger volumes. The octahedral cation sequences in these nonstandard structures are always ordered and usually form more complex ordered arrays than in the standard polytypes, e.g., I,I,II and I,I,II,II, etc. The stacking of layers may be random or regular. The interlayer stacking sequences of the regular-stacking varieties are explained only by intermixing of zero and $\pm$**b**/3 interlayer shifts or by mixing of $-$**b**/3 and $+$**b**/3 shifts in patterns other than alternating $-,+,-,+$, etc. Most can be described by triclinic-shaped unit cells with $\alpha \neq 90°$, although some of these can also be described by tripling the number of layers to form a rhombohedral structure with $\alpha = 90°$, and some are based on orthogonal axes.

The $6R_2$ polytype (treated here as two-layer triclinic) is locally abundant, and one three-layer and four four-layer regular-stacking polytypes occur less often. To identify the latter precisely, it was necessary to make a theoretical computer derivation of all polytypes that are possible with any combination of zero, $+$**b**/3, and $-$**b**/3 interlayer shifts and any combination of I and II octahedral cation sets occupied along **c**. Long-period, ordered octahedral cation sequences up to seven layers were also observed but always with random interlayer stacking for octahedral periodicities greater than four layers.

We present here the derivation of all nonstandard, regular-stacking interlayer sequences up to four layers (a total of 14) and the diffraction characteristics that identify each uniquely. We present also all the possible octahedral cation sequences up to seven layers and their diffraction criteria. The numbers of the remaining stacking and octahedral sequences up to nine layers are given, but their diffraction patterns are not presented. The specific nonstandard serpentines encountered in our own studies, their occurrences, and their origins will be reported separately (Banfield et al., 1995).

We calculated diffraction patterns for both X-ray and electron diffraction. Dynamical scattering effects expected for a sample thickness of 32 Å were incorporated in the electron diffraction patterns, and it should be noted that Friedel's Law is not necessarily obeyed in the calculated patterns, and that reflections for which the calculated intensities are zero may actually be observed because of dynamical scattering.

General principles

Bailey (1988) pointed out that the octahedral cations and anions within a 1:1 layer repeat at intervals of **b**/3 and thus diffract exactly in phase with one another for all reflections with index $k = 3n$, which are generally strong as a result. The periodicity between adjacent reflections of this type ($20l$ and $13l$ are most convenient) on single-crystal or powder patterns is the same as the periodicity between identical octahedral sheets in the structure. For the standard polytypes, groups A and C have 7 Å periodicity and groups B and D have 14 Å periodicity between identical octahedral sheets. For polytypes within the same group, all reflections with $k = 3n$ indices have identical intensities, provided the compositions are similar.

Table 1. The α values for the n-layer triclinic-shaped models

$n =$	1	2	3	4	5	6	7
Net $-$**b**/3 shift (°)	113.35	102.18	98.19	96.16	94.93	94.11	93.53
Net $-$2**b**/3 shift (°)	130.80	113.35	106.05	102.18	99.80	98.19	97.03

Table 2. Model characteristics for *n*-layer regular-stacking serpentines

Model	*n*	Interlayer shifts	Octahedral sequence	α (°)	Space group	Identifying characteristics
1	2	0,−	I,II	102.18	*C*1	$I(l$ = odd) > $I(l$ = even) for 02*l*
2	3	0,+,+	all I,I,II	98.19	*C*1	020 strong
3	3	−,−,+	all I,I,II	98.19	*C*1	021 and 02$\bar{2}$ strong
4	3	0,0,−	all I,I,II	98.19	*C*1	022 and 02$\bar{1}$ strong
5	3	0,−,+	I,I,II	90	*C*1	all 02*l* intensities similar
6	4	0,0,0,−	either I,II,I,II, I,I,I,II, or I,I,II,II	96.16	*C*1	023 and 02$\bar{1}$ strong
7	4	+,+,+,−		96.16	*C*1	021 and 02$\bar{3}$ strong
8	4	0,−,−,+		96.16	*C*1	022 and 02$\bar{2}$ strong
9	4	0,−,+,−		96.16	*C*1	020 missing
10	4	0,0,+,+		96.16	*C*1	020 strong
11	4	−,−,+,+	either I,II,I,II, I,I,I,II, or I,I,II,II	90	*Cc**	022 and 02$\bar{2}$ strong
12	4	0,−,0,+		90	*Cc**	022 and 02$\bar{2}$ missing
13	4	0,0,−,+		90	*C*1	020 strong
14	4	0,−,−,−		90	*C*1	023 and 02$\bar{1}$ strong

* Monoclinic *Cc* with a I,II,I,II octahedral cation sequence. The **a** and **b** axes are reversed in model 12 but not in model 11.

The tetrahedral cations repeat at intervals of **b**/3, but the periodicity is interrupted by the center of each six-membered ring. The basal O atoms do not repeat at intervals of **b**/3. Both of these atom types contribute to all reflections, but they are the only contributors to intensities of the $k \neq 3n$ reflections, which are generally weak as a consequence. The periodicity between adjacent $k \neq 3n$ reflections (02*l* and 11*l* are most convenient, using a *C*-centered orthogonal base for indexing) is the same as the repeat between identical basal O planes in the structure, which can differ in position according to the interlayer shifts present. The $k \neq 3n$ reflections, therefore, identify the polytypes within each of the four groups of standard polytypes. Figure 2 shows that the repeat between octahedral cation planes is not necessarily the same as the repeat between basal O planes. All these general principles can be applied equally well to the nonstandard polytypes that are derived in the present paper.

The simplifying assumptions in the present derivation are as follows: (1) The 1:1 layers are planar and identical in composition and structure. (2) The octahedral sheets are trioctahedral with no vacancies. (3) No cation ordering takes place. (4) The tetrahedral and octahedral sheets have undistorted hexagonal geometry. (5) The stacking of layers is regular rather than random. (6) Only interlayer shifts of zero and $\pm$**b**/3 are permitted. Because shifts along $\mathbf{b}_1$, $\mathbf{b}_2$, and $\mathbf{b}_3$ do not give rise to different polytypes, only shifts along $\mathbf{b}_1$ are used. Symbols 0, −, and + are used to designate interlayer shifts of zero, −**b**/3, and +**b**/3, respectively. (7) Any combination of occupancy of the I and II sets of octahedral positions in different layers is permitted. (8) Orthorhombic-, monoclinic-, and triclinic-shaped unit cells are considered. The triclinic-shaped unit cells have $\beta = \gamma = 90°$ but $\alpha \neq 90°$.

In accordance with the recommendation of Hall et al. (1976), polytype symbols are not given to these theoretical structures. They are called models until such time as they are known to exist. The method of derivation and the terminology used are those of Bailey (1969).

The composition assumed for calculation of the different diffraction patterns is $Mg_3Si_2O_5(OH)_4$. The cell dimensions are $a = 5.323$, $b \sin \alpha = 9.220$, $c \sin \alpha = 7.120$ Å $\times$ *n*, $\beta = \gamma = 90°$ with α variable. The α values used for the *n*-layer triclinic-shaped models are given in Table 1 and explained as follows. For a given *n* value, say 4, the diffraction pattern could be indexed with either $\alpha = 96.16°$ or $\alpha = 102.18°$ by choosing the **b*** row line on a **b*-c*** diffraction pattern to go on opposite sides of the line corresponding to $\alpha^* = 90°$. All our indexing is based on a resultant −**b**/3 shift. Observed intensities may be expected to deviate somewhat from the calculated values because of compositional or distortional differences, but the differences are not considered great enough to prevent identification (see below). Table 2 lists the interlayer shifts and octahedral cation sequences for all models, and Appendix Table 1 lists their calculated 20*l* and 02*l* X-ray intensities to facilitate identification. Table 3 lists the atomic coordinates for all regular stacking models.[1] All reflections are indexed on a *C*-centered orthohexagonal base.

The diagnostic reflections used to identify the interlayer stacking sequences are of type 02*l* and 11*l*, and the 02*l* intensities may or may not be equivalent to those of 11*l*. The equivalence relations for reflection intensities for each model are listed in Appendix Table 1. When the crystallographic angle $\alpha \neq 90°$, the three pseudohexagonal reciprocal zone axes [010]*, [110]*, and [1$\bar{1}$0]* do not make the same angle with the zone axis [001]*. It is not possible to determine which of these three reciprocal zone axes is present along with [001]* in a given SAED pattern, however, because the overall distribution of intensities remains similar for all three cases. But the following identification rule is applicable to all our calculated models. Assume that each apparent **b*-c*** SAED pattern represents true **b*-c*** and, therefore, that the first row lines on either side of **c*** are true 02*l* and 02$\bar{l}$ reflections (rather than 11*l* and 11$\bar{l}$ or 1$\bar{1}$*l* and 1$\bar{1}\bar{l}$). Table 2 summarizes the

[1] A copy of Table 3 may be ordered as Document AM-95-599 from the Business Office, Mineralogical Society of America, 1015 Eighteenth Street NW, Suite 601, Washington, DC 20036, U.S.A. Please remit $5.00 in advance for the microfiche.

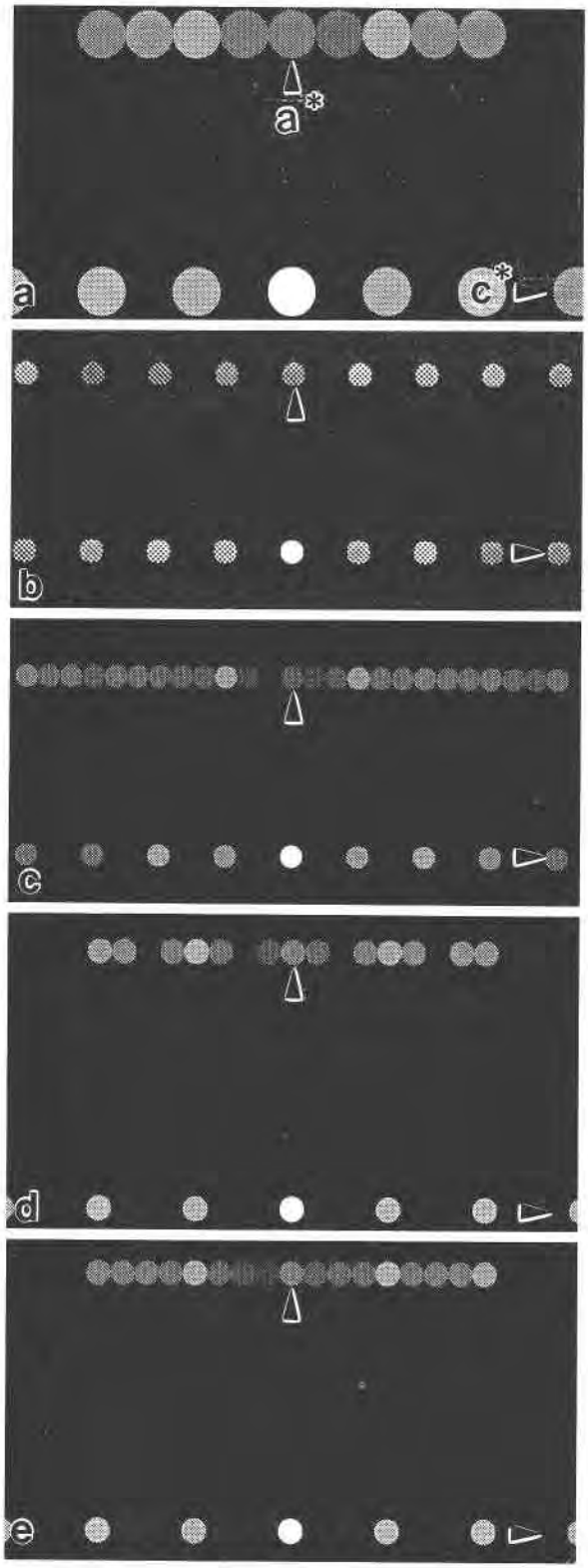

Fig. 3. Calculated [010] SAED patterns for octahedral cation sequences. (**a**) I,II,I,II, (**b**) I,I,I, (**c**) I,I,II, (**d**) I,I,II,II, and (**e**) I,I,I,II. These patterns are not affected by the nature of the interlayer stacking sequences. The calculations incorporate dynamical scattering effects expected for a sample thickness of 32 Å.

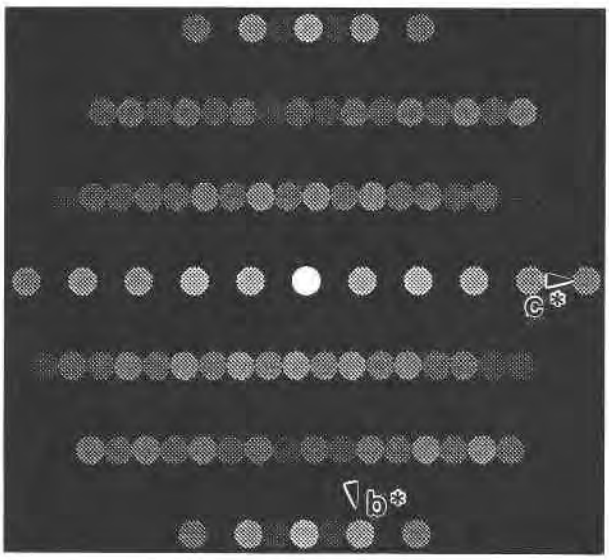

Fig. 4. Calculated [100] SAED pattern for the $6R_2$ polytype. The [110] and [1$\bar{1}$0] patterns are indistinguishable from that of [100]. Note that for the intensities of 0*kl* reflections with indices $l \neq 3n$, l = odd is more intense than l = even.

identifying features for each model on the basis of which 02*l* and 02$\bar{l}$ reflections are either strong or missing. It does not matter which of the three reciprocal zone axes is actually present. The same reasoning applies to the distinction between the pseudohexagonal 20*l*, 13*l*, and 1$\bar{3}$*l* reflections. It should be assumed that each apparent **a*-c*** SAED pattern represents true **a*-c***, and the intensities for the 20*l* and 20$\bar{l}$ reflections listed in Appendix Table 1 should be used to differentiate the octahedral cation sequences.

Octahedral cation sequences

In our specimens the octahedral cations always form an ordered sequence along **c**, whereas the interlayer shifts may be either regular or random. When the layer stacking is regular, the periodicity between identical basal O planes is either the same as or a multiple of the periodicity between identical octahedral cation planes. For two- and three-layer polytypes the only possible octahedral cation sequences along **c** (excluding I,I,I) are I,II and I,I,II, respectively. Three sequences are possible in four-layer polytypes, namely I,II,I,II and I,I,I,II and I,I,II,II, or permutations thereof. The periodicity between adjacent 20*l* reflections is 14 Å for I,II and I,II,I,II and 21 Å for I,I,II. Both I,I,I,II and I,I,II,II sequences have 28 Å periodicities, and the calculated intensities (Appendix Table 1) must be used for differentiation. Both give strong 20*l* reflections for $l = 4n$, but the I,I,II,II sequence also has absences for $l = 4n \pm 2$. Calculated SAED patterns for all these octahedral cation sequences are illustrated in Figure 3. Octahedral Fe, replacing Mg, increases the intensities of the 20*l* reflections as a general rule but not necessarily in a proportional manner. Calculated values for the octahedral cation sequences above show that the

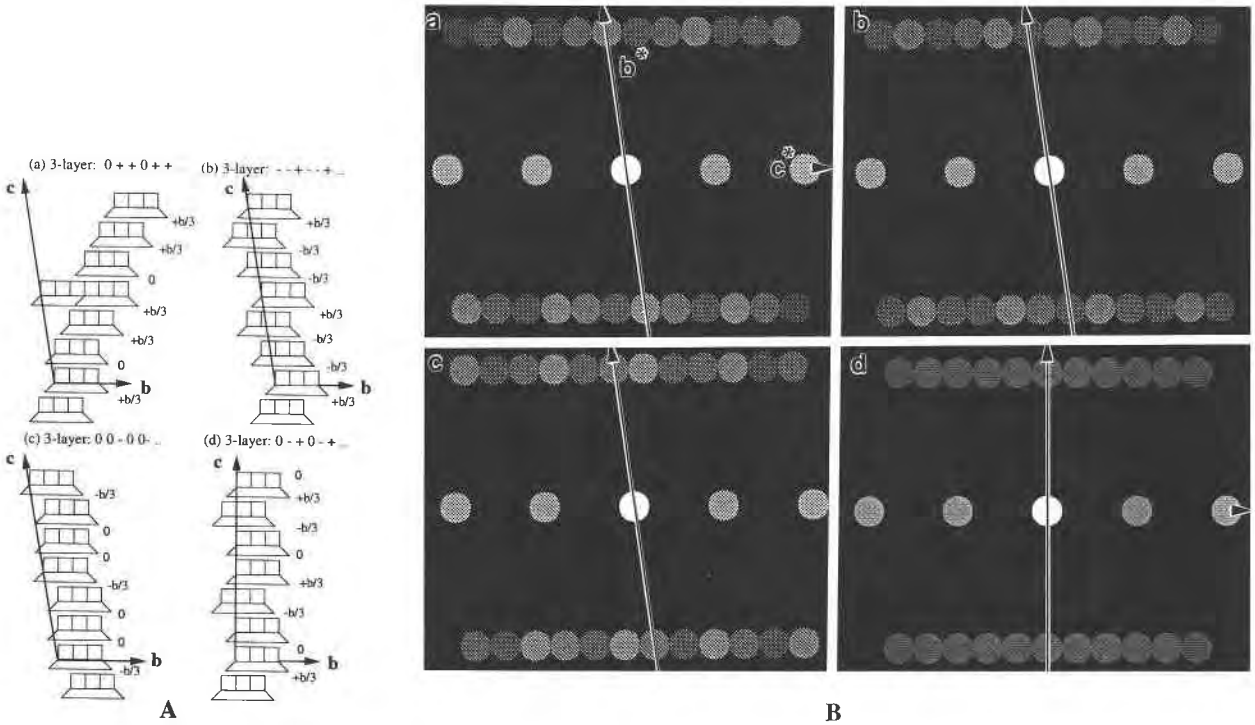

Fig. 5. (**A**) Possible stacking sequences and (**B**) calculated [100] SAED patterns for three-layer serpentines with $\alpha = 98°$: (**a**) 0,+,+, (**b**) −,−,+, (**c**) 0,0,−, and with $\alpha = 90°$: (**d**) 0,−,+. The position of the strong 02*l* reflection is different in calculated patterns for the three models with triclinic-shaped unit cells but occurs in the same position relative to the 82° reciprocal angle α^* in the [100], [110], and [1$\bar{1}$0] zones for a specific stacking sequence (see text). Calculations incorporate dynamical scattering effects expected for a sample thickness of 32 Å. Intensity differences are apparent in samples up to ~10 nm thick.

patterns of intensities listed in Appendix Table 1 are equally valid for the Mg and Fe end-members, and this is true also for all octahedral cation sequences reported in this paper.

Equivalence relationships

Equivalence relationships of all interlayer stacking sequences reported in this paper were considered. In an interlayer stacking sequence along **c** such as 0,0,0,−, for example, 0,0,0,− = 0,0,−,0 = 0,−,0,0 = −,0,0,0 because this simply moves the origin to a different layer along the sequence and does not change the diffraction pattern. Reversing the sequence to −,0,0,0 generates identical sequences. For other sequences, a reversal may generate equivalent rather than identical patterns. This equivalency was built into our computer program. The same equivalence of forward and reverse sequences holds also for the octahedral cation sequences. For example, I,I,I,II = I,I,II,I = I,II,I,I = II,I,I,I. This means that the origin within any sequence is indeterminant and, thus, that the precise location of the II octahedral set in a I,I,I,II sequence or the −**b**/3 shift in a 0,0,0,− sequence cannot be determined by these methods. It is tempting, however, to assume that a change in stacking mode is coupled with a change in the octahedral cation set occupancy, and most of our calculated patterns were modeled in this manner.

Two-layer regular polytypes

Only one model is possible that gives an offset of −**b**/3 per two layers, namely a shift sequence of 0,− (or 0,−**b**/3) to give an α angle of 102°. If the octahedral cations alternate regularly (i.e., I,II) and the layer stacking pattern is extended to six layers, this is the already recognized $6R_2$ polytype of symmetry $R3$ with $\alpha = 90°$. Known examples in amesite and cronstedtite actually have triclinic symmetry as a consequence of cation ordering, and so the smaller two-layer cell is preferable. Polytype $2Tc$ (= $6R_2$) is identified by alternately weak and medium intensities of the 02*l* and 02$\bar{l}$ reflections, with l = odd more intense than l = even (Fig. 4 and Appendix Table 1). Comparison with intensities calculated from the atomic coordinates of Wiewióra et al. (1991) for the $2Tc$ structure of amesite from Poland, in which there is considerable distortion because of tetrahedral rotation and cation ordering, shows that the ratio between the intensities of adjacent medium to weak 02*l* reflections decreases from an average of 2.76 in the ideal structure to 2.20 in the actual structure. But the pattern of medium and weak adjacent reflections is still discernible. Substitution of 50% $^{[4]}$Fe in the same distorted structure (as in cronstedtite) returns the ratio to 2.74. The same effects are found for the calculated and observed patterns for the standard $2H_2$ polytype of amesite, which has very similar intensity differences between

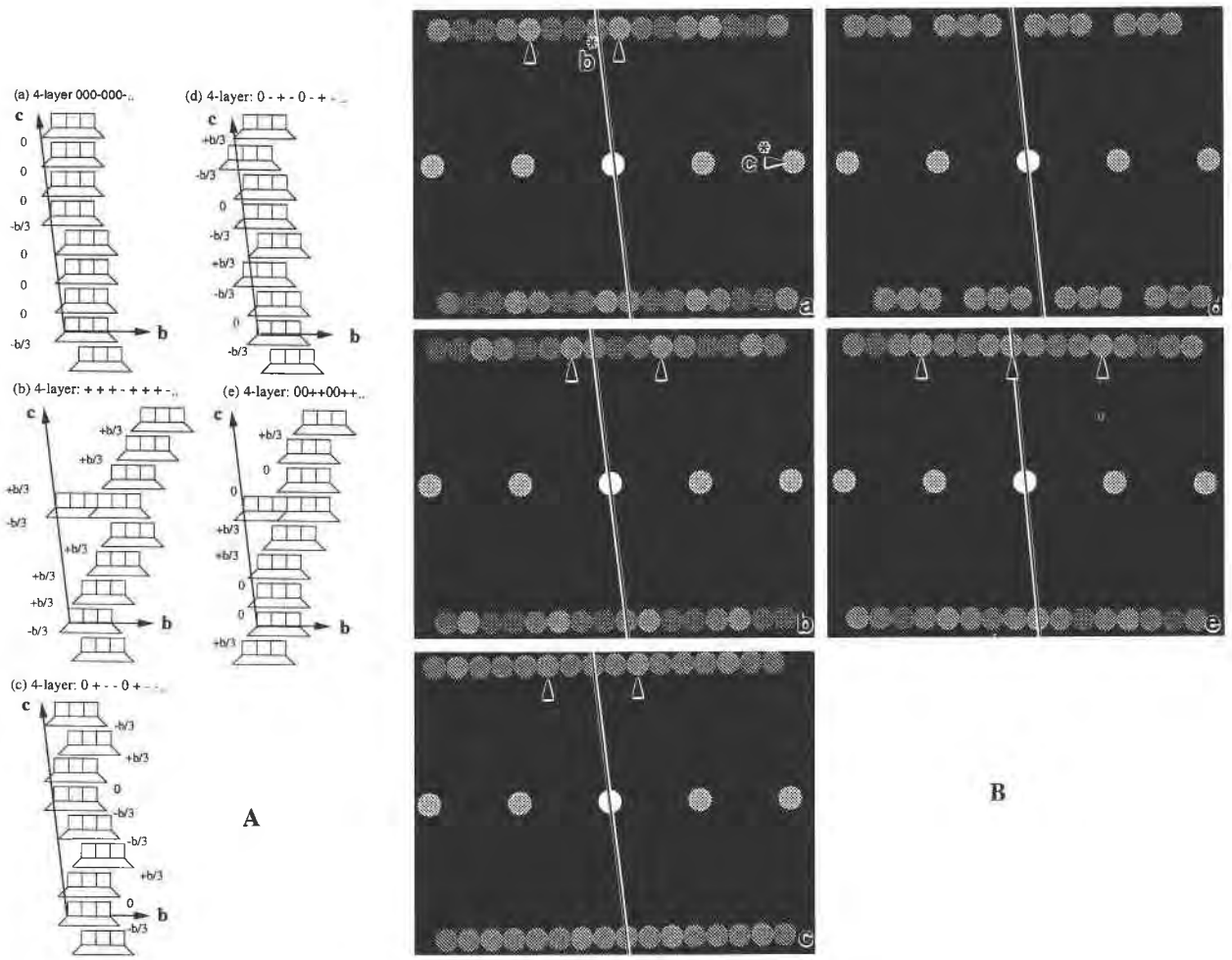

Fig. 6. (**A**) Possible stacking sequences and (**B**) calculated [100] SAED patterns for serpentines with four-layer periodicities in 0*kl* reflections with $k \neq 3n$ and $\alpha = 96°$: (**a**) 0,0,0,−, (**b**) +,+,+,−, (**c**) 0,+,−,− (equivalent to 0,−,−,+), (**d**) 0,−,+,−, and (**e**) 0,0,+,+. The position of the strong or missing 02*l* reflection relative to the 84° reciprocal angle is different for each structure but the same in the [100], [110], and [1$\bar{1}$0] zones for a single structure (see text). Calculations incorporate dynamical scattering effects expected for a sample thickness of 32 Å.

adjacent 02*l* reflections. As mentioned previously, compositional differences in the octahedral cations affect only the $k = 3n$ reflections, and then only the magnitudes of the intensities are affected rather than the periodicity between adjacent reflections. So the stacking sequence present in an Fe-, Ni-, or Co-bearing serpentine can be identified as readily as in the Mg species. If the octahedral cations were all in the same set of positions in every layer of a 0,−**b**/3 stacking sequence, then the $k \neq 3n$ reflections would remain unchanged from those in the 2*Tc* structure, but the $k = 3n$ reflections would have only a 7 Å periodicity between adjacent reflections (instead of 14 Å as in 2*Tc*, see Fig. 3). The $2M_2$ standard polytype with interlayer shifts of ±**a**/3 also has a comparable 102° angle and the same I,II octahedral cation sequence as in 2*Tc*, but it can be recognized by its monoclinic distribution of intensities and the reversal of the customary **a** and **b** axes.

Three-layer regular polytypes

Four stacking variants are possible: 0,+,+; −,−,+; 0,0,−; and 0,−,+. The first three models are based on unit cells with $\alpha = 98°$, and the last is based on orthogonal axes but has triclinic symmetry (Table 2). Models 0,+,+ and 0,0,− have rhombohedral symmetry *R*3 if extended to nine layers. The only possible ordered octahedral cation sequence along **c** that gives a three-layer repeat is I,I,II (= I,II,I = II,I,I).

Figure 5A illustrates the stacking sequences possible for three-layer models. Figure 5B shows the calculated electron diffraction patterns for these models. The identification rules cited in Table 2 can be applied as follows: first (upper) pattern 020 strong = 0,+,+ sequence, second pattern 021 strong = −,−,+ sequence, and third pattern 022 strong = 0,0,− sequence. The lower pattern for mod-

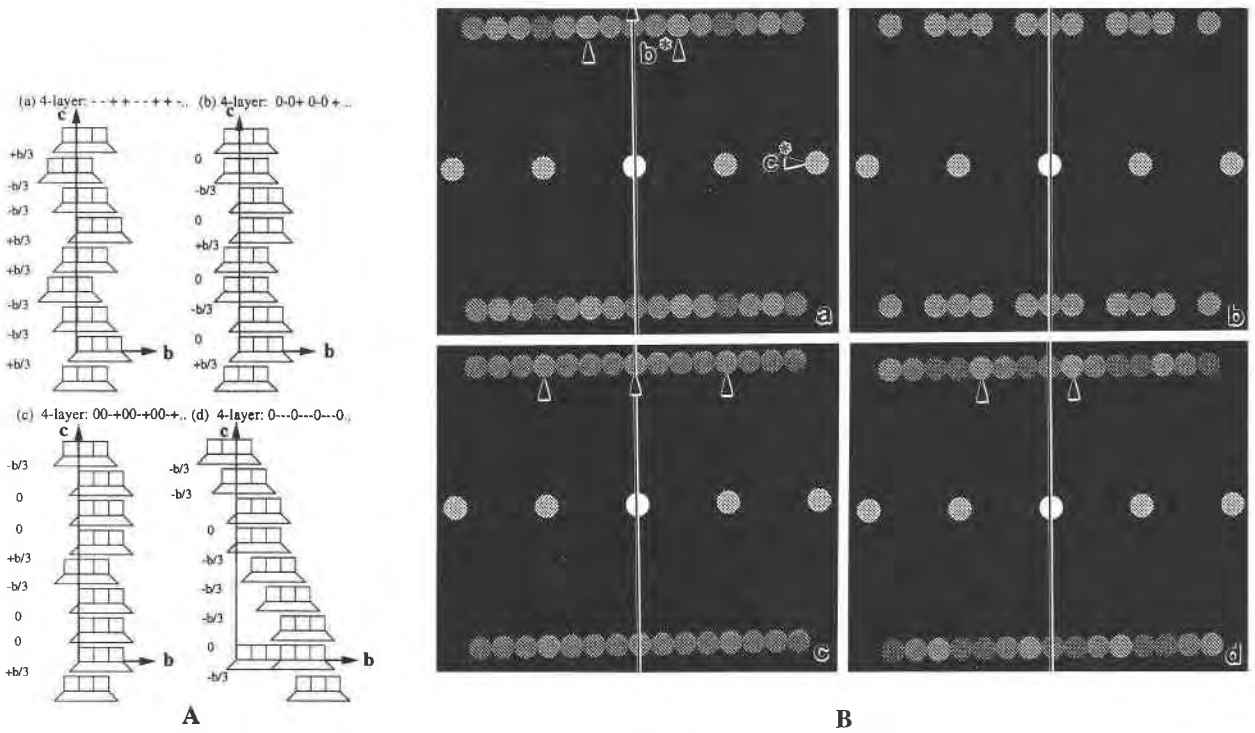

Fig. 7. (**A**) Possible stacking sequences and (**B**) calculated [100] SAED patterns for serpentines with four-layer regular stacking and $\alpha = 90°$ that produce four-layer periodicities in $0kl$ reflections with $k \neq 3n$: (**a**) $-,-,+,+$, (**b**) $0,-,0,+$, (**c**) $0,0,-,+$, and (**d**) $0,-,-,-$. The position of the strong or missing $02l$ reflection is different in each calculated pattern but the same in the [100], [110], and [$1\bar{1}0$] zones for each structure. Calculations incorporate dynamical scattering effects expected for a sample thickness of 32 Å.

el 5 with a $0,-,+$ interlayer shift sequence and orthogonal axes gives $02l$ intensities that are all similar. It should be noted that the intensities listed in Appendix Table 1 are based on X-ray scattering factors for the elements. The calculated intensities illustrated in the figures, however, are based on electron scattering and incorporate dynamical scattering effects expected for a sample thickness of 32 Å. The thickness at which dynamical diffraction becomes sufficiently intense to obscure the intensity differences among the polytypes of this study varies. In most cases (e.g., for $2Tc$), we found that the characteristic intensity criteria remain apparent to thicknesses in excess of 100 Å. The results of our study of natural specimens (Banfield et al., 1995) verify that the calculated and observed electron diffraction intensities are comparable for suitably thin and well-oriented specimens.

Four-layer regular polytypes

We observed both triclinic- and monoclinic-symmetry SAED patterns from serpentines that have four-layer periodicity in the $02l$ reflections. Five interlayer stacking sequences give rise to a unit cell with $\alpha = 96°$, namely $0,0,0,-$; $+,+,+,-$; $0,-,-,+$; $0,-,+,-$; and $0,0,+,+$. The identification criteria (Table 2) are as follows: The most intense reflection in the $02l$ row line is 020 for $0,0,+,+$, 021 for $+,+,+,-$, 022 for $0,-,-,+$, and 023 for $0,0,0,-$. For the $0,-,+,-$ sequence, the criterion is that 020 is absent. Figure 6A and 6B illustrate the five models and their calculated SAED patterns.

There are four possible models that give a four-layer periodicity in which the axes are orthogonal ($\alpha = 90°$),

Table 4. Model characteristics for long-period octahedral cation sequences

Model	n	Octahedral sequence	Identification criteria
1	5	I,I,I,I,II	201, 202, 203, 204 similar intensities
2	5	I,I,II,II,II	201, 204 strong
3	5	I,II,I,II,I	202, 203 strong
1	6*	I,I,I,I,I,II	201, 202, 203, 204, 205 similar intensities
2	6	I,I,II,II,II,II	203 absent
3	6	I,II,I,II,II,II	203 strong
4	6	I,I,I,II,II,II	202, 204 absent
5	6	I,I,II,I,II,II	202, 204 strong
1	7	I,I,I,I,I,I,II	201, 202, 203, 204, 205, 206 similar intensities**
2	7	I,I,II,II,II,II,II	203, 204 weak
3	7	I,I,I,II,II,II,II	201, 206 strong
4	7	I,II,I,II,II,II,II	202, 205 weak
5	7	I,II,II,I,II,II,II	201, 206 weak
6	7	I,II,I,I,II,II,II	201, 202, 203, 204, 205, 206 similar intensities**
7	7	I,II,II,I,I,II,II	202, 205 strong
8	7	I,II,I,II,I,II,II	201, 202 and 205, 206 weak

* The pattern for I,I,II,I,I,II is the same as for the three-layer repeat I,I,II (listed in Appendix Table 1 and illustrated in Fig. 3).
** See text for identification.

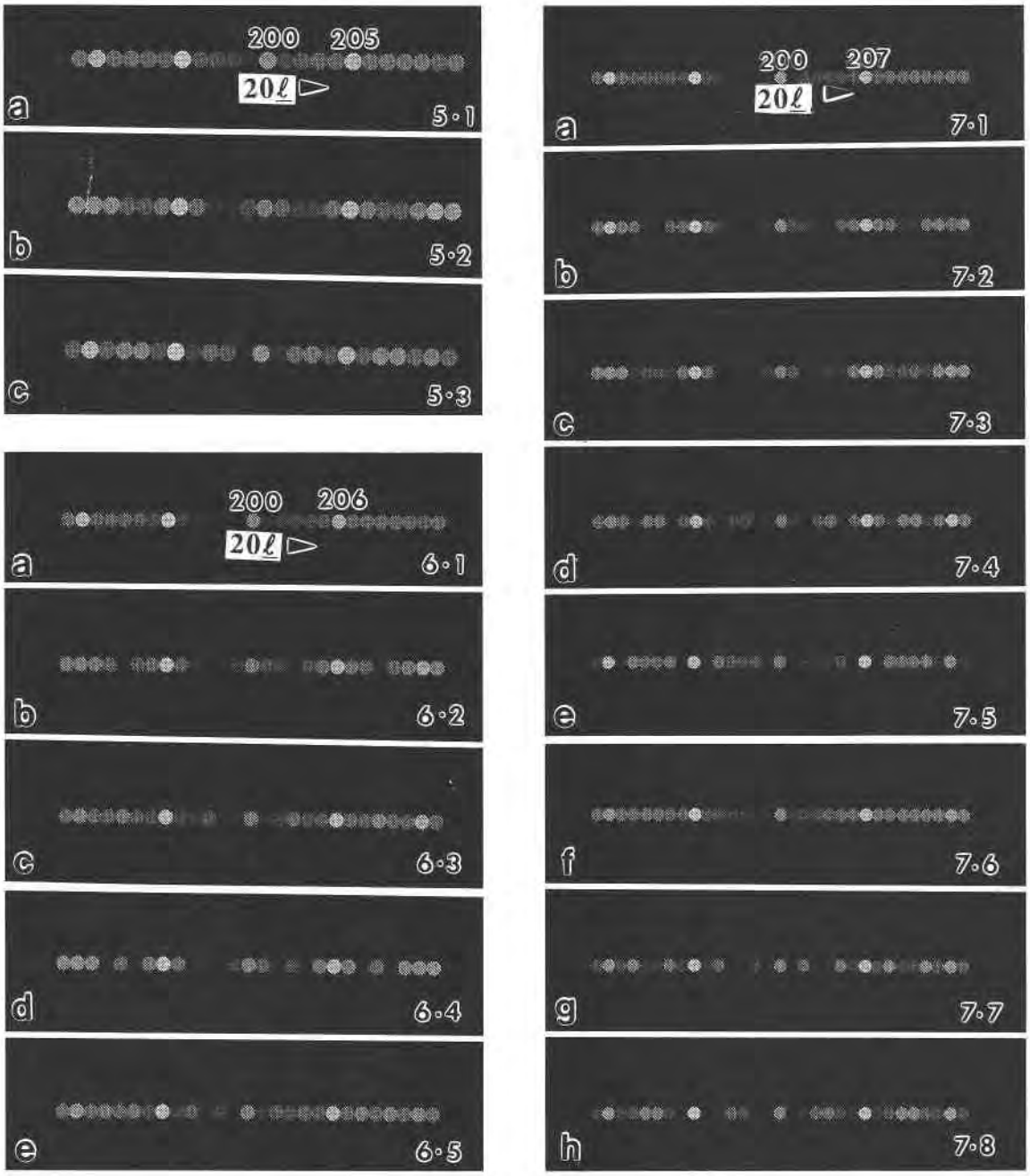

Fig. 8. Calculated [010] SAED patterns for five-, six-, and seven-layer octahedral cation sequences. Only the 20*l* row lines are shown. Labels such as 5·1 indicate the pattern for the five-layer repeat, model 1 octahedral cation sequence listed in Table 4.

namely stacking sequences −,−,+,+; 0,−,0,+; 0,0,−,+; and 0,−,−,−. The sequence 0,−,0,+ in model 12 has monoclinic symmetry *Cc* with **a** and **b** reversed but only if the octahedral cation sequence is I,II,I,II. Otherwise, the symmetry is *C*1. Model 11 also has *Cc* symmetry if the octahedral cation sequence is I,II,I,II, but in this case the axes are not reversed. Figure 7A and 7B illustrate the four models and their calculated patterns.

The nine regular, four-layer, interlayer stacking sequences can each exist with any of the following three octahedral cation sequences: I,II,I,II; I,I,I,II; or I,I,II,II. This creates 27 four-layer polytypes. The interlayer stacking sequences and the octahedral cation sequences are identified by the intensities of the 02*l* and 20*l* reflections, respectively, as listed in Appendix Table 1.

Long-period sequences

There are three possible five-layer, six six-layer, eight seven-layer, 16 eight-layer, and 22 nine-layer nonstandard, ordered, octahedral cation sequences along **c** (ex-

cluding I,I, etc. and I,II, etc.). Table 4 lists the sequences and the identification criteria for the five-, six-, and seven-layer cases. Figure 8 shows their calculated SAED patterns. Appendix Table 2 lists the calculated $20l$ intensities on which the identification criteria are based. Identification usually can be made from the weaker $20l$ intensities by observing whether selected reflections are medium, weak, or absent. The only exception is the seven-layer sequences where the $20l$ intensities for reflections with indices $l \neq 7n$ are similar for models $7\cdot1$ and $7\cdot6$. The $l = 7n$ intensities are different for the two models, however, so identification can be made by noting that the ratio $F^2(20l)/F^2(20l)$ for $l = 7n$ pairs is greater for model $7\cdot1$ than for model $7\cdot6$ (Appendix Table 2). The diffraction patterns for the eight- and nine-layer cases were not calculated.

The number of possible nonstandard, regular-stacking, interlayer shift sequences increases rapidly with an increasing number of layers. There are 20 possible five-layer sequences (including eight with orthogonal axes), 44 six-layer sequences (17 with orthogonal axes), 104 seven-layer sequences, 253 eight-layer sequences, and 624 nine-layer sequences. The enormity of the possibilities can be better appreciated by noting for a given layer repeat, say $n = 7$, that each of the 104 regular-stacking models can exist with any of eight different ordered octahedral cation sequences for a total of 728 seven-layer models. It is questionable whether many of these will be found to exist, and we did not calculate diffraction patterns for $n > 4$.

Hybrid standard polytypes

It is also possible, at least on a theoretical basis, to have the same interlayer stacking sequences present in the standard polytypes but with more complex octahedral cation sequences. For example, the interlayer shift sequence $-,-,-$, etc., as in $3R$, or 0,0,0,0, etc., as in $1T$, could exist with various octahedral cation sequences, perhaps I,I,II in $3R$ and I,I,I,II in $1T$. In such cases, the interlayer shift sequences can be identified according to the tables for the standard polytypes given by Bailey (1969), and the octahedral cation sequences can be identified by the $20l$ intensities given in Appendix Table 1 of the present paper. In the reverse sense, it is possible also to have nonstandard, regular interlayer stacking sequences but standard octahedral cation sequences (cations all in the same set of positions in every layer or alternating I,II). The I,II sequence is especially common for the serpentines we studied (e.g., in specimens with four-layer regular interlayer shift sequences).

Conclusions

Many nonstandard serpentine polytypes are theoretically possible. These are based on regular interlayer stacking sequences and ordered octahedral cation sequences along **c** that were not considered in the original derivations of the standard polytypes. The polytypes derived here are identified based on both electron and X-ray diffraction intensities and the periodicities between adjacent reflections. Specifically, in the case of electron diffraction, the relative intensities of selected $20l$ and $02l$ reflections are definitive providing that suitably thin and well-oriented specimens are employed. Calculations and comparisons with well-refined structures show that the distortional and compositional differences to be expected in natural analogs of these ideal structures are not great enough to prevent identification.

Acknowledgments

This research was supported by NSF grant EAR-9117386 to J.F.B. and by a grant from the Department of Geology and Geophysics, University of Wisconsin–Madison, to S.W.B. We are indebted to Lee Powell for devising the computer programs used to generate octahedral cation and interlayer shift models.

References cited

Anderson, C.S., and Bailey, S.W. (1981) A new cation ordering pattern in amesite-$2H_2$. American Mineralogist, 66, 185–195.

Bailey, S.W. (1969) Polytypism of trioctahedral 1:1 layer silicates. Clays and Clay Minerals, 17, 355–371.

——— (1988) X-ray diffraction identification of the polytypes of mica, serpentine, and chlorite. Clays and Clay Minerals, 36, 193–213.

Banfield, J.F., Bailey, S.W., Barker, W.W., and Smith, R.C., II (1995) Complex polytypism: Relationships between serpentine structural characteristics and deformation. American Mineralogist, 80, 1116–1131.

Dornberger-Schiff, K., and Ďurović, S. (1975a) OD-interpretation of kaolinite-type structures: Symmetry of kaolinite packets and their stacking possibilities. Clays and Clay Minerals, 23, 219–229.

——— (1975b) OD-interpretation of kaolinite-type structures: The regular polytypes (MDO-polytypes) and their derivation. Clays and Clay Minerals, 23, 231–246.

Ďurović, S., Miklos, D., and Dornberger-Schiff, K. (1981) Polytypism of kaolinite-type minerals: An aid to visualize the stacking of layers. Crystal Research and Technology, 16, 557–565.

Hall, S., Guggenheim, S., Moore, P., and Bailey, S.W. (1976) The structure of Unst-type 6-layer serpentines. Canadian Mineralogist, 14, 314–321.

Jahanbagloo, I.C., and Zoltai, T. (1968) The crystal structure of a hexagonal Al-serpentine. American Mineralogist, 53, 14–24.

Steadman, R. (1964) The structures of trioctahedral kaolin-type silicates. Acta Crystallographica, 17, 924–927.

Steadman, R., and Nuttall, P.M. (1962) The crystal structure of amesite. Acta Crystallographica, 15, 510–511.

——— (1963) Polymorphism in cronstedtite. Acta Crystallographica, 16, 1–8.

——— (1964) Further polymorphism in cronstedtite. Acta Crystallographica, 17, 404–406.

Wiewióra, A., Rausell-Colom, J.A., and García-González, T. (1991) The crystal structure of amesite from Mount Sobotka: A nonstandard polytype. American Mineralogist, 76, 647–652.

Zheng, H., and Bailey, S.W. (1995) Refinement of an amesite-$2H_1$ polytype from Postmasburg, South Africa. Clays and Clay Minerals, in press.

Zussman, J., and Brindley, G.W. (1957) Electron diffraction studies of serpentine minerals. American Mineralogist, 42, 133–153.

Zvyagin, B.B. (1962) Polymorphism of double-layer minerals of the kaolinite type. Soviet Physics-Crystallography, 7, 38–51 [translated from Kristallografiya, 7(1), 51–65, 1962].

Zvyagin, B.B., Mishchenko, K.S., and Shitov, V.A. (1966) Ordered and disordered polymorphic varieties of serpentine-type minerals and their diagnosis. Soviet Physics-Crystallography, 10, 539–546 [translated from Kristallografiya, 10(5), 635–643, 1965].

Manuscript received August 4, 1994
Manuscript accepted June 23, 1995

Appendix Table 1. Calculated intensities F^2 ($\times 10^{-3}$) for regular-stacking serpentine models

	Octahedral cation sequences							Interlayer stacking sequences								
				Four-layer				Two-layer, $\alpha = 102°$ $2Tc_1$ (=$6R_2$) (0,−)		Three-layer, $\alpha = 98°$						Three-layer, $\alpha = 90°$
	Two-layer	Three-layer								Model 2 (0,+,+)		Model 3 (−,−,+)		Model 4 (0,0,−)		Model 5 (0,−,+)
l	I,II	I,I,II		I,II,I,II	I,I,I,II		I,I,II,II									
	20l	20l	20$\bar{l}$	20l	20l	20$\bar{l}$	20l	02l	02$\bar{l}$	02l	02$\bar{l}$	02l	02$\bar{l}$	02l	02$\bar{l}$	02l
0	1.1	2.6	—	4.3	5.1	—	4.3	1.5	—	8.5	—	1.0	—	2.4	—	4.1
1	1.5	1.1	1.1	0	1.0	1.0	1.9	3.5	4.0	2.3	1.0	8.1	2.4	1.0	8.6	4.0
2	15.7	2.1	2.1	6.1	1.5	1.5	0	1.0	1.4	0.9	2.4	2.1	8.3	7.3	1.0	3.7
3	6.0	47.3	25.2	0	2.5	2.5	4.9	2.1	3.0	6.3	7.6	0.8	0.9	1.8	2.2	3.3
4	4.0	5.2	5.2	62.7	95.7	36.9	62.7	0.5	0.8	1.5	0.8	5.3	1.9	0.6	6.7	2.8
5	8.4	6.6	6.6	0	4.8	4.8	9.5	1.0	1.6	0.5	1.6	1.2	5.7	4.3	0.7	2.3
6	3.0	16.7	5.0	23.8	5.9	5.9	0	0.2	0.4	3.4	4.6	0.4	0.6	1.0	1.3	1.9
7	6.5	8.4	8.4	0	7.0	7.0	13.9	0.4	0.7	0.8	0.4	2.7	1.0	0.3	3.7	1.5
8	7.2	8.4	8.4	15.7	38.8	7.9	15.7	0.1	0.2	0.2	0.8	0.6	2.9	2.0	0.4	1.1
9	3.2	16.0	1.4	0	8.1	8.2	16.3	0.1	0.2	1.5	2.2	0.2	0.3	0.4	0.6	0.8
10	2.7	7.1	7.1	33.5	8.3	8.3	0	0	0.1	0.1	1.6	0.3	0.2	1.0	0.5	0.6

Equivalencies

Two layer, $\alpha = 102°$: $F^2(20l) = F^2(20\bar{l}) \approx F^2(\bar{1}3l) \approx F^2(1\bar{3}l) \approx F^2(13\bar{l}) \approx F^2(13l)$

Three layer, $\alpha = 98°$: $F^2(20l) = F^2(13\overline{l+1}) = F^2(\bar{1}3l - 1) \neq F^2(20\bar{l}) = F^2(13l - 1) = F^2(1\bar{3}l + 1)$

Three layer, $\alpha = 90°$: $F^2(20l) = F^2(13\bar{l}) = F^2(\bar{1}3l) \neq F^2(20\bar{l}) = F^2(1\bar{3}l) = F^2(13l)$

Four layer, $\alpha = 96°$:

(I,II,I,II) and (I,I,II,II): $F^2(20l) = F^2(20\bar{l}) = F^2(\bar{1}3l) = F^2(1\bar{3}l) = F^2(13\bar{l}) = F^2(13l)$

(I,I,I,II): $F^2(20l) = F^2(13\overline{l+1}) = F^2(\bar{1}3l - 1) \neq F^2(20\bar{l}) = F^2(13l - 1) = F^2(1\bar{3}l + 1)$

Four layer, $\alpha = 90°$:

(I,II,I,II) and (I,I,II,II): $F^2(20l) = F^2(20\bar{l}) = F^2(\bar{1}3l) = F^2(1\bar{3}l) = F^2(13\bar{l}) = F^2(13l)$

(I,I,I,II): $F^2(20l) = F^2(13\bar{l}) = F^2(\bar{1}3l) \neq F^2(20\bar{l}) = F^2(1\bar{3}l) = F^2(13l)$

Equivalencies

Two layer, $\alpha = 102°$: $F^2(02l) = F^2(11\overline{l+1}) = F^2(1\bar{1}l + 1) \neq F^2(02\bar{l}) = F^2(11l - 1) = F^2(\bar{1}1l - 1)$

Three layer, $\alpha = 98°$: $F^2(02l) = F^2(11\overline{l+1}) = F^2(1\bar{1}l + 1) \neq F^2(02\bar{l}) = F^2(11l - 1) = F^2(\bar{1}1l - 1)$

Three layer, $\alpha = 90°$: $F^2(02l) = F^2(11\bar{l}) = F^2(1\bar{1}l) = F^2(02\bar{l}) = F^2(11l) = F^2(\bar{1}1l)$

Appendix Table 2. Calculated intensities F^2 ($\times 10^{-3}$) for long-period octahedral sequences

	Five-layer						Six-layer									
	Model 5·1 (I,I,I,I,II)		Model 5·2 (I,I,II,II,II)		Model 5·3 (I,II,I,II,I)		Model 6·1 (I,I,I,I,I,II)		Model 6·2 (I,I,II,II,II,II)		Model 6·3 (I,II,I,II,II,II)		Model 6·4 (I,I,I,II,II,II)		Model 6·5 (I,I,II,I,II,II)	
l	20l	20$\bar{l}$	20l	20$\bar{l}$	20l	20$\bar{l}$	20l	20$\bar{l}$	20l	20$\bar{l}$	20l	20$\bar{l}$	20l	20$\bar{l}$	20l	20$\bar{l}$
0	8.4	—	6.9	—	6.9	—	12.7	—	10.4	—	10.4	—	9.7	—	9.7	—
1	0.9	0.9	2.3	2.3	0.3	0.3	0.8	0.8	2.5	2.5	0.8	0.8	3.4	3.4	0.8	0.8
2	1.3	1.3	0.5	0.5	3.3	3.3	1.1	1.1	1.1	1.1	1.1	1.1	0	0	3.3	3.3
3	1.9	1.9	0.7	0.7	4.9	4.9	1.5	1.5	0	0	6.2	6.1	1.6	1.6	1.5	1.5
4	2.6	2.6	7.0	7.0	1.0	1.0	2.1	2.1	2.1	2.1	2.1	2.1	0	0	6.4	6.4
5	161.3	50.9	80.5	117.4	117.3	80.5	2.8	2.8	8.4	8.4	2.8	2.8	11.3	11.3	2.8	2.8
6	4.6	4.6	11.9	11.8	1.7	1.7	243.8	67.1	100.2	189.3	100.4	189.0	140.8	141.4	141.0	141.2
7	5.5	5.5	2.1	2.1	14.3	14.4	4.5	4.5	13.2	13.1	4.4	4.4	17.6	17.5	4.4	4.4
8	6.4	6.3	2.4	2.4	16.7	16.8	5.2	5.2	5.2	5.2	5.1	5.1	0	0	15.6	15.7
9	7.0	7.2	18.7	18.7	2.8	2.7	6.0	5.9	0	0	24.0	23.8	6.1	6.0	6.0	6.1
10	71.5	12.9	16.8	36.6	36.4	16.9	6.7	6.7	6.6	6.5	6.6	6.7	0	0	20.1	20.0
11	8.2	8.2	21.4	21.3	3.1	3.1	7.2	7.3	21.9	21.8	7.4	7.3	29.1	29.1	7.1	7.1
12	8.4	8.3	3.3	3.2	21.8	21.9	113.6	19.8	19.8	67.4	19.8	67.1	35.4	36.0	35.7	35.6
13	8.4	8.4	3.2	3.2	22.1	22.0	8.2	8.3	24.5	24.1	8.2	8.1	32.6	32.3	8.2	8.1
14	8.1	8.2	21.5	21.4	3.2	3.1	8.3	8.3	8.5	8.4	8.1	8.2	0	0	25.1	25.1
15	72.7	0.2	8.5	32.8	32.7	8.5	8.5	8.3	0	0	33.9	33.5	8.6	8.4	8.4	8.6
16	7.4	7.5	19.6	19.4	2.8	2.7	8.4	8.4	8.2	8.2	8.4	8.5	0	0	25.1	25.1
17	6.8	6.9	2.6	2.7	17.8	17.9	8.1	8.2	24.8	24.4	8.3	8.2	32.9	32.7	8.0	8.0
18	6.2	6.2	2.4	2.3	16.2	16.5	115.8	0.4	5.5	63.5	5.5	63.4	26.4	26.6	26.5	26.5
19	5.4	5.5	14.4	14.3	2.2	2.1	7.6	7.7	22.7	22.3	7.6	7.4	30.2	29.9	7.7	7.5
20	37.8	73.5	51.8	40.3	40.1	52.0	7.0	7.0	7.2	7.2	6.8	7.1	0	0	21.1	21.3
21	4.1	4.2	10.8	10.8	1.6	1.5	6.6	6.4	0	0	26.3	25.9	6.6	6.4	6.4	6.6

APPENDIX TABLE 1.—*Continued*

	Four-layer, α = 96°										Four-layer, α = 90°				
	Model 6 (0,0,0,−)		Model 7 (+,+,+,−)		Model 8 (0,−,−,+)		Model 9 (0,−,+,−)		Model 10 (0,0,+,+)		Model 11 (−,−, +,+)	Model 12 (0,−, 0,+)	Model 13 (0,0, −,+)	Model 14 (0,−,−,−)	
l	$02l$	$02\bar{l}$	$02l$	$02\bar{l}$	$02l$	$02\bar{l}$	$02l$	$02\bar{l}$	$02l$	$02\bar{l}$	$02l$	$02l$	$02l$	$02l$	$02\bar{l}$
0	4.0	—	4.0	—	4.0	—	0	—	12.1	—	1.4	5.4	9.5	1.4	—
1	1.1	15.1	14.6	1.1	3.9	4.1	7.8	8.1	3.9	4.1	4.0	8.0	4.0	1.1	14.9
2	1.2	1.3	1.2	1.3	8.6	9.2	4.9	5.3	1.2	1.3	11.5	0	3.8	3.8	3.8
3	12.7	1.0	0.9	14.2	3.4	3.8	6.8	7.5	3.4	3.8	3.6	7.2	3.6	13.4	1.0
4	3.0	3.5	3.1	3.5	3.1	3.5	0	0	9.2	10.5	1.1	4.4	7.6	1.1	1.1
5	0.7	11.8	10.0	0.8	2.7	3.2	5.3	6.3	2.7	3.2	2.9	5.8	2.9	0.8	10.9
6	0.8	0.9	0.8	1.0	5.4	6.5	3.1	3.7	0.8	0.9	7.7	0	2.6	2.6	2.6
7	7.2	0.6	0.5	9.0	2.0	2.4	3.9	4.9	2.0	2.4	2.2	4.4	2.2	8.2	0.6
8	1.7	2.0	1.6	2.0	1.6	2.1	0	0	4.9	6.2	0.6	2.5	4.3	0.6	0.6
9	0.4	6.6	5.1	0.5	1.4	1.7	2.8	3.5	1.4	1.7	1.6	3.1	1.6	0.4	5.8
10	0.4	0.5	0.4	0.5	2.6	3.4	1.5	1.9	0.4	0.5	3.9	0	1.3	1.3	1.3

Equivalencies

Four layer, α = 96°: $F^2(02l) = F^2(11\overline{l+1}) = F^2(1\bar{1}l+1) \neq F^2(02\bar{l}) = F^2(11l-1) = F^2(\bar{1}1l-1)$

Equivalencies

Model 12: $F^2(02l) = F^2(11\bar{l}) = F^2(1\bar{1}l) \neq F^2(02\bar{l}) = F^2(11l) = F^2(\bar{1}1l)$

Models 11, 13, and 14: $F^2(02l) = F^2(11\bar{l}) = F^2(1\bar{1}l) = F^2(02\bar{l}) = F^2(11l) = F^2(\bar{1}1l)$

APPENDIX TABLE 2.—*Continued*

	Seven-layer															
	Model 7·1 (I,I,I,I,I,I,II)		Model 7·2 (I,I,II,II,II,II,II)		Model 7·3 (I,I,I,II,II,II,II)		Model 7·4 (I,II,I,II,II,II,II)		Model 7·5 (I,II,II,I,II,II,II)		Model 7·6 (I,II,I,I,II,II,II)		Model 7·7 (I,II,II,I,I,II,II)		Model 7·8 (I,II,I,II,I,II,II)	
l	$20l$	$20\bar{l}$	$20l$	$20\bar{l}$	$20l$	$20\bar{l}$	$20l$	$20\bar{l}$	$20l$	$20\bar{l}$	$20l$	$20\bar{l}$	$20l$	$20\bar{l}$	$20l$	$20\bar{l}$
0	17.9	—	14.8	—	13.3	—	14.8	—	14.8	—	13.3	—	13.3	—	13.3	—
1	0.8	0.8	2.6	2.6	4.1	4.1	1.3	1.3	0.2	0.2	1.6	1.6	0.5	0.5	0.3	0.3
2	1.0	1.0	1.6	1.6	0.3	0.3	0.2	0.2	3.3	3.3	2.0	2.0	5.1	5.1	0.6	0.6
3	1.3	1.3	0.3	0.3	0.8	0.8	4.3	4.3	2.1	2.1	2.7	2.6	0.4	0.4	6.7	6.7
4	1.8	1.8	0.3	0.3	1.1	1.1	5.8	5.7	2.7	2.7	3.5	3.5	0.5	0.5	8.9	8.9
5	2.3	2.3	3.6	3.6	0.7	0.7	0.5	0.5	7.5	7.5	4.6	4.6	11.6	11.6	1.5	1.5
6	2.9	2.9	9.5	9.5	14.7	14.7	4.5	4.5	0.6	0.6	5.8	5.8	1.9	1.9	0.9	0.9
7	343.3	85.8	122.9	277.6	167.3	218.9	123.0	277.4	123.0	277.4	167.4	218.7	167.3	218.8	167.3	218.8
8	4.2	4.3	13.9	13.8	21.6	21.5	6.7	6.7	0.8	0.8	8.6	8.6	2.7	2.8	1.3	1.3
9	5.0	4.9	7.7	7.7	1.5	1.5	1.0	1.0	16.1	16.1	9.9	9.9	25.0	25.0	3.2	3.1
10	5.6	5.7	1.1	1.1	3.6	3.6	18.2	18.2	8.8	8.8	11.1	11.2	1.7	1.7	28.4	28.3
11	6.2	6.3	1.2	1.2	4.1	4.1	20.3	20.4	9.6	9.7	12.5	12.5	1.9	1.9	31.6	31.6
12	6.7	6.7	10.6	10.6	2.1	2.1	1.4	1.4	22.3	22.1	13.8	13.7	34.6	34.4	4.4	4.3
13	7.3	7.4	23.8	23.8	36.9	36.9	11.4	11.4	1.4	1.4	14.6	14.7	4.7	4.7	2.3	2.3
14	165.3	28.5	24.8	107.1	36.8	64.1	24.9	106.9	24.8	107.0	36.8	64.0	36.6	64.3	36.7	64.2
15	8.0	8.1	26.2	26.1	40.8	40.7	12.6	12.6	1.6	1.6	16.2	16.2	5.2	5.2	2.5	2.5
16	8.4	8.3	13.0	12.8	2.6	2.6	1.6	1.6	26.9	26.9	16.5	16.5	41.8	41.7	5.3	5.2
17	8.4	8.4	1.7	1.6	5.4	5.4	27.1	27.1	13.0	13.0	16.6	16.6	2.6	2.6	42.3	42.3
18	8.4	8.4	1.6	1.6	5.4	5.4	27.3	27.3	13.0	13.0	16.8	16.8	2.6	2.6	42.2	42.4
19	8.2	8.2	12.9	12.9	2.5	2.5	1.7	1.7	27.1	26.9	16.8	16.7	42.1	41.9	5.4	5.3
20	8.2	8.2	26.4	26.4	40.9	40.9	12.6	12.6	1.6	1.6	16.2	16.2	5.2	5.2	2.5	2.5
21	170.6	1.3	3.5	105.2	21.6	55.5	3.5	105.1	3.5	105.1	21.6	55.4	21.6	55.5	21.6	55.5